JACS
JOURNAL OF THE AMERICAN CHEMICAL SOCIETY

Article

pubs.acs.org/JACS

Influence of Molecular Structure on the Properties of Out-of-Equilibrium Oscillating Enzymatic Reaction Networks

Albert S. Y. Wong, Sjoerd G. J. Postma, Ilia N. Vialshin, Sergey N. Semenov,[†] and Wilhelm T. S. Huck*

Radboud University, Institute for Molecules and Materials, Heyendaalseweg 135, 6525 AJ Nijmegen, The Netherlands

Supporting Information

ABSTRACT: Our knowledge of the properties and dynamics of complex molecular reaction networks, for example those found in living systems, considerably lags behind the understanding of elementary chemical reactions. In part, this is because chemical reactions networks are nonlinear systems that operate under conditions far from equilibrium. Of particular interest is the role of individual reaction rates on the stability of the network output. In this research we use a rational approach combined with computational methods, to produce complex behavior (in our case oscillations) and show that small changes in molecular structure are sufficient to impart large changes in network behavior.

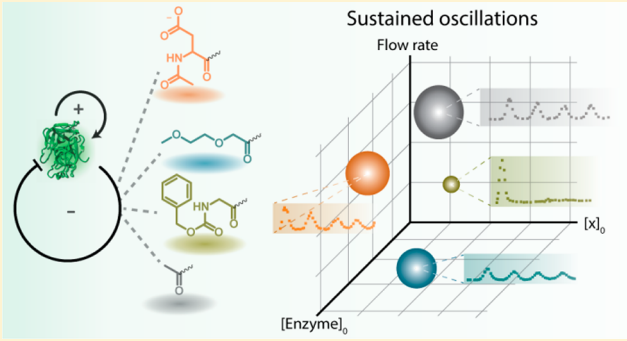

INTRODUCTION

Enzymatic chemical reaction networks (CRNs) drive many of the key processes in living systems, including circadian clocks, signaling pathways, energy metabolism, and cell division.[1,2] Interactions and feedback loops within CRNs give rise to dynamic and complex behavior.[3] A classic example of complex behavior in out-of-equilibrium conditions are oscillations.[4,5] The general design principles behind the oscillatory behavior are well-understood, and the network topologies required to produce a certain behavior are known.[6−9] Inspired by examples in synthetic biology,[10,11] recent studies in dynamic self-assembly systems[12−14] and cell-free gene circuits[15,16] have highlighted the potential for constructing reaction networks with designed outputs. However, they also show that subtle changes in substituents in key components have a profound influence on the observed behavior of a system. The key challenges encountered in the experimental realization of a robust steady-state output are often associated with balancing of reaction rates between various feedback loops in the network. Sometimes, these rates are not known, or cannot be tuned easily, as is often the case in for example synthetic gene networks. Nevertheless, even for oscillators with equal topologies, differences in their regulatory components result in different network properties. These differences can lead to changes in the characteristic periods of the oscillators from minutes to hours but could also shift the regime in which sustained oscillations can be found.[1,7]

Now, to gain insight in how the molecular structure influences the behavior of out-of-equilibrium complex systems, we employ a bottom-up approach where parts of the network can be tuned, while keeping all other rates constant. This work is based on our recently described strategy to design enzymatic CRNs capable of producing limit cycle oscillations.[17] In our network, autocatalytic production of the enzyme trypsin is coupled to a delayed negative feedback loop regulated by small organic molecules. In contrast to other oscillators such as those based on DNA circuits,[18−20] reconstituted cellular networks,[21,22] or inorganic compounds,[23−26] the enzymatic oscillator can be disassembled to study elementary reactions, and the use of small molecules allows tunability and control over individual components of the system by organic synthesis.

Here, we exploit the flexibility introduced by using small synthetic peptides as key intermediates in the enzymatic network, by synthesizing a range of compounds that change one reaction rate, and one rate only, in a specific part of the network by an order of magnitude. Due to the nonlinear nature of the CRN, this change in reaction rate in one part of the network will not lead to a corresponding linear change in output of the network (i.e., amplitude or periodicity). Instead, it will change the very nature of the steady state behavior. In this work, we combine experiments with computational methods to follow these changes in the network upon the introduction of different small molecules.

RESULTS AND DISCUSSION

Enzymatic Reaction Network. Our oscillatory network consists of four main enzymatic reactions: autocatalysis, activation, delay, and inhibition (Figure 1). The central enzyme trypsin (Tr), a mammalian endopeptidase, cleaves amide bonds on the carboxylic side of lysine residues.[27,28] In the short positive feedback loop, Tr converts its own inactive precursor trypsinogen (Tg) in an autocatalytic way. The delayed negative feedback loop ultimately results in inhibition of Tr, but the

Received: August 10, 2015
Published: September 9, 2015

DOI: 10.1021/jacs.5b08129
J. Am. Chem. Soc. 2015, 137, 12415−12420

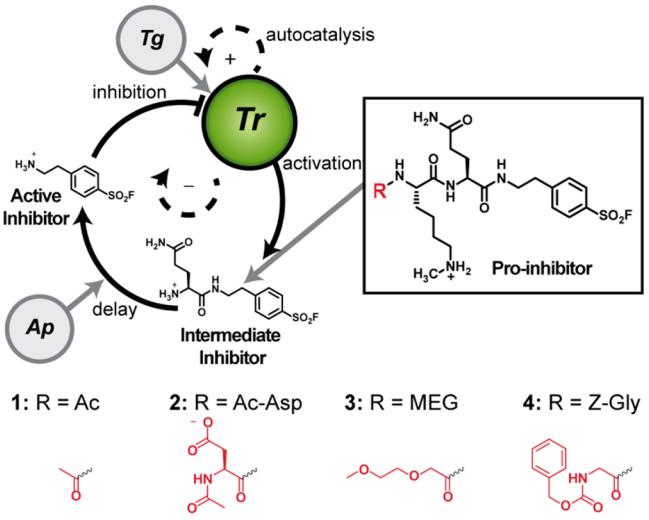

Figure 1. Enzymatic reaction network with R-modified pro-inhibitors: acetyl (Ac, **1**), acetylated aspartic acid (Ac-Asp, **2**), methoxy ethylene glycol (MEG, **3**), and carboxybenzyl-protected glycine (Z-Gly, **4**). The structures **1**−**4** are synthesized by a combination of conventional solid-phase and solution-phase peptide chemistry (see Supporting Information ESI-S2).

recognition of the potent, active inhibitor (4-(2-aminoethyl)-benzenesulfonyl fluoride, AEBSF)[29] is initially hampered by amino acid residues. In the activation step, Tr converts a pro-inhibitor into an intermediate inhibitor, which consists of a glutamine (Gln) residue attached to the inhibitor moiety. Please note that we use methylated lysine residues in the pro-inhibitor to slow down the rate of activation.[17,30] Cleavage of Gln in the delay step is controlled by aminopeptidase N (Ap) and yields the active inhibitor that closes the negative feedback loop.

By modifying the N-termini of the pro-inhibitors, we can selectively influence the rate of pro-inhibitor cleavage by Tr in the activation step (see Figure 1). In addition to the earlier reported acetyl derivative (Ac, **1**), we synthesized three more analogues with different R-groups: acetylated aspartic acid (Ac-Asp, **2**), methoxy ethylene glycol (MEG, **3**), and carboxybenzyl-protected glycine (Z-Gly, **4**). Since trypsin preferably hydrolyses peptide bonds at nonterminal sites, we expect the neutral Z-Gly residue to enhance the trypsin affinity toward the pro-inhibitor. Conversely, the acidic Ac-Asp residue is expected to slow down the rate of trypsin hydrolysis.[31] MEG was selected as a neutral side-group of increased size compared to the acetyl group.

Enzymatic conversions of all compounds were investigated using kinetic studies, in which unavoidable background reactions (hydrolysis of the sulfonyl fluorides and background inhibition of trypsin by pro-inhibitor) were all taken into account (see ESI-S3). The rate constants of the activation step are shown in Table 1, in which k_{act} is a measure for the specificity of Tr toward the pro-inhibitor. Notably, the background reactions are similar for all compounds (see ESI-S3). The kinetic studies show that the values of k_{act} differ significantly between compounds **1**−**4**, ranging from 21 to 482 mM^{-1} h^{-1}, and that the activation rate increases in the following series: **2** < **3** < **1** < **4**.

Structure−Network Property Relations. Subsequently, we used a computational bifurcation analysis (Figure 2a) to screen the effect of changes in k_{act} values on the properties of

Table 1. Experimentally Determined Activation Rates

pro-inhibitor	R-group	activation rate k_{act} (mM^{-1} h^{-1})[a]
1	acetyl	47
2	Ac-Asp	21
3	MEG	28
4	Z-Gly	482

[a]Activation rate, $k_{act} = k_{cat}/K_M$. See ESI-S3 for details.

the CRN. This analysis is based on the set of ordinary differential equations (ODEs) we used previously to describe our network.[17] Here, we are interested in finding a range of k_{act} values for which the method predicts two possible solutions for [Tr], indicative of an oscillatory regime.[32] Indeed, the analysis shows that the k_{act} values of pro-inhibitors **1**−**4** all fall within the calculated oscillatory regime (Figure 2a, dotted lines). Furthermore, the diagram indicates that the amplitudes of the predicted sustained oscillations associated with each of the four molecules (Figure 2a, arrows) follow the reverse trend found in the activation rates of **1**−**4**: **4** > **1** > **3** > **2**.

Next, we tested the properties of **1**−**4** experimentally in the full network under batch conditions (in which case an equilibrium state is inevitably reached). Figure 2b shows that the reaction network gives an initial rise in [Tr] for each of the pro-inhibitors, before decaying to equilibrium in which trypsin is fully inhibited by the inhibitor freed in solution. The observed single oscillations in [Tr] differ in period and amplitude, which decrease both upon increasing k_{act} values. A slower activation of the negative feedback loop allows a longer buildup of trypsin, leading to higher amplitudes. Consequently, these oscillations die out with longer periods compared to the CRN with **4**, where much less trypsin is activated in the first place. However, there appears to be no clear linear relationship between k_{act} and the period or the amplitude of the single oscillations. The batch experiments provide early evidence that subtly changing the molecular structure of the pro-inhibitor significantly alters the quantitative behavior of the full network, consistent with the trend found in the bifurcation analysis.

Then, to allow the system to oscillate continuously, we implemented flow using a poly(dimethylsiloxane) (PDMS)-based continuous stirred tank reactor (CSTR) to create out-of-equilibrium conditions.

We performed the reaction in flow conditions that based on previous work should result in so-called limit cycle oscillations.[17,33] As shown in Figure 2c, these oscillations are characterized by a sustained behavior when the CRN contains pro-inhibitor **1**. After an initial period of stabilization, [Tr] oscillates between 1.0 and 8.3 μM.

To our surprise, the flow experiments conducted under similar conditions resulted in qualitatively different behavior for CRNs with **2**−**4**. Even though the first peaks in flow conditions follow the same trend as in batch experiments, it appears that when **1** was substituted by **2**, **3**, or **4**, neither a decrease nor an increase in activation rate resulted in sustained oscillations. The [Tr] oscillations for **2**−**4** were damped and ended in different steady states ($[Tr]_{SS}$ = 9.7 μM for **2**, 4.8 μM for **3**, and 0.2 μM for **4**). In contrast to the predicted range of activation rates in the bifurcation diagram, the experiments in Figure 2c suggest that in reality the oscillating range is smaller.

Enzymatic Reaction Network Characteristics. The precise correlation between molecular structure and balance of reaction rates in the network that causes this discrepancy between calculated and experimental bifurcation remains

DOI: 10.1021/jacs.5b08129
J. Am. Chem. Soc. 2015, 137, 12415−12420

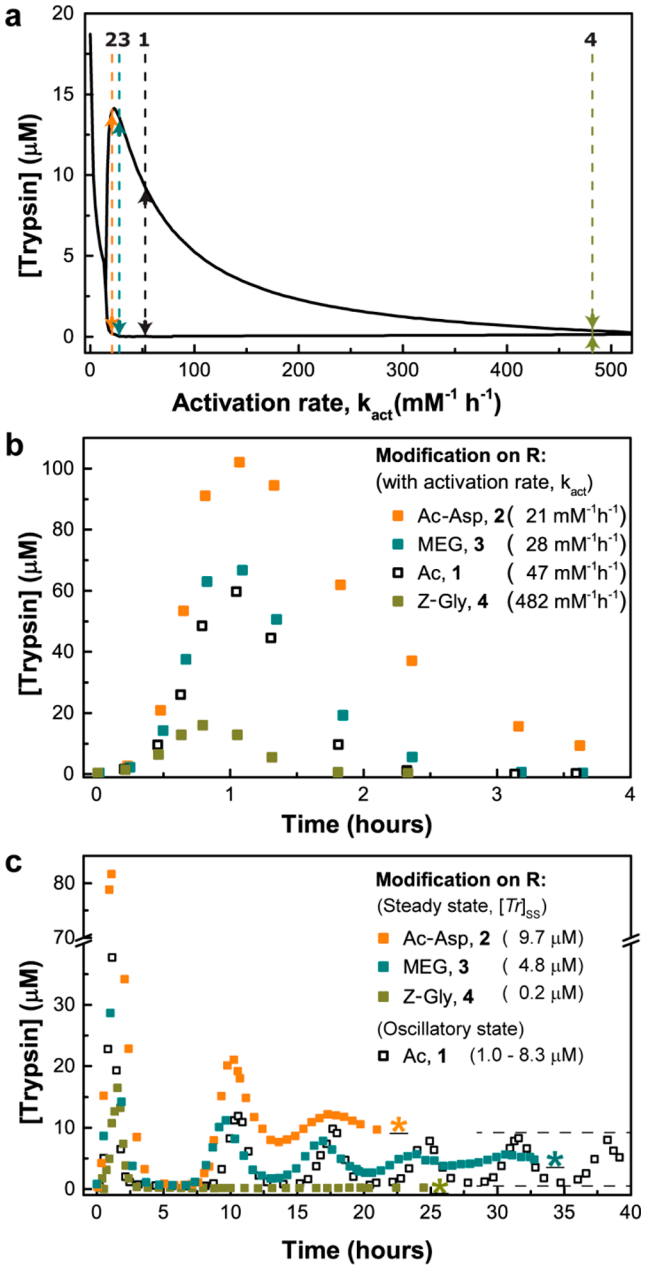

Figure 2. Structure–property relations observed in (a) bifurcation diagram of the CRN. The phase diagram is constructed from 300 simulated time series in which k_{act} was varied from 0 to 500 mM^{-1} h^{-1} (see ESI-S4 for full details). The diagram describes the dynamical behavior of the CRN, by summarizing the state (steady state or oscillatory) of each simulated time series. According to (a), **1**–**4** should all oscillate with the peak-to-peak amplitudes of [Tr] marked by the corresponding colored arrows. (b) Experimentally obtained time series under batch conditions for CRNs with **1**–**4**. (c) Experimentally obtained time series obtained in out-of-equilibrium conditions for CRNs with **1**–**4**, with end states marked as either being a steady state (colored stars) or oscillatory state (dashed line).

unclear. The flow experiments do, however, highlight that changes in molecular structure and corresponding reaction rates do not translate to the network properties in a linear fashion.

To investigate which parameters in our network need to be tuned in order to obtain the desired sustained oscillations for CRNs containing pro-inhibitors **2**–**4**, we screened a range of initial pro-inhibitor concentrations, $[\mathbf{x}]_0$ (**x** = **2**, **3**, or **4**), initial aminopeptidase concentrations $[Ap]_0$, and flow rates by computational simulations. The mathematical model, with the specific rate constants for **2**–**4**, was used to construct three-dimensional (3D) phase plots shown in Figure 3. Essentially, the 3D phase plots predict the experimental conditions under which oscillations are expected to be found, in a similar way as the bifurcation diagram in Figure 2a. Figure 3 shows that sustained oscillations are predicted for pro-inhibitors **2**–**4**, with especially large regimes for pro-inhibitors **2** (Figure 3a) and **3** (Figure 3b). Although the predicted phase plots in Figure 3 could be smaller in reality (like the bifurcation diagram in Figure 2a), the shapes of the oscillatory regimes and positions in the 3D space are substantially different. This indicates that minor changes in molecular structure of the pro-inhibitor alter the characteristics of the whole network, as sustained oscillations will be found at different conditions.

Re-establishing Sustained Oscillating Behavior. The results in Figure 3 provide a route to find new sets of conditions for each pro-inhibitor to re-establish sustained oscillating behavior. Figure 4a depicts an example of the procedure followed to select new conditions using the 3D phase plot for pro-inhibitor **1**. Slices of the 3D plot in the (flow, [Ap])-plane are taken, and the relative area of the oscillatory regime is calculated by a computer script. Figure 4b shows the dependency of the size of (flow, Ap)-parameter space giving oscillatory regimes plotted against $[\mathbf{x}]_0$. Instead of looking for the highest amplitude, these calculations rather yield the largest regime (equivalent to the highest probability of finding the desired behavior). Clearly, each pro-inhibitor has a different profile, and crucially, the apparent optimal $[\mathbf{x}]_0$ (i.e., the concentration pro-inhibitor giving the largest parameter space with sustain oscillations) differs for each pro-inhibitor. Additional graphs are reported in ESI-S5 to show improvements of the phase plots in (flow, Ap)-plane at optima for **2**–**4**.

To test our model predictions, we performed experiments with $[\mathbf{x}]_0$ (**x** = **2**, **3** or **4**), $[Ap]_0$ and flow conditions retrieved from the screening procedure in Figure 4. The time series for **2** and **3** (orange and cyan squares in Figure 5a and 5b, respectively) show clear improvement in the oscillations when compared to the corresponding initial flow experiments from Figure 2c (gray squares). Under the new conditions, the CRN containing **2** shows sustained oscillations between 5 and 11 μM, while the one containing pro-inhibitor **3** oscillates between 1 and 3 μM. Although the resulting oscillations can be categorized as similar behavior, the actual oscillations are different, judged by the peak-to-peak amplitude and periods. The predicted oscillatory regime in the case of pro-inhibitor **4** is very small and reaches peak-to-peak amplitudes barely above the baseline of 2.5 μM (green trace, Figure 3c). Perhaps not unexpectedly, we were unable to find limit cycle oscillations within the predicted parameter range (Figure 5c).

CONCLUSION

In this work, we studied the properties of an oscillating enzymatic reaction network composed of one positive and one negative feedback loop. Of particular interest was the change in network properties upon changes in one of the reaction rates in the negative feedback loop. We synthesized a range of four pro-inhibitors, each with slightly different affinities for the key enzyme in our CRN. These four molecules gave a distinct trend in activation rates of the negative feedback loop. Our experiments showed that changing reaction rates in one part

DOI: 10.1021/jacs.5b08129
J. Am. Chem. Soc. 2015, 137, 12415–12420

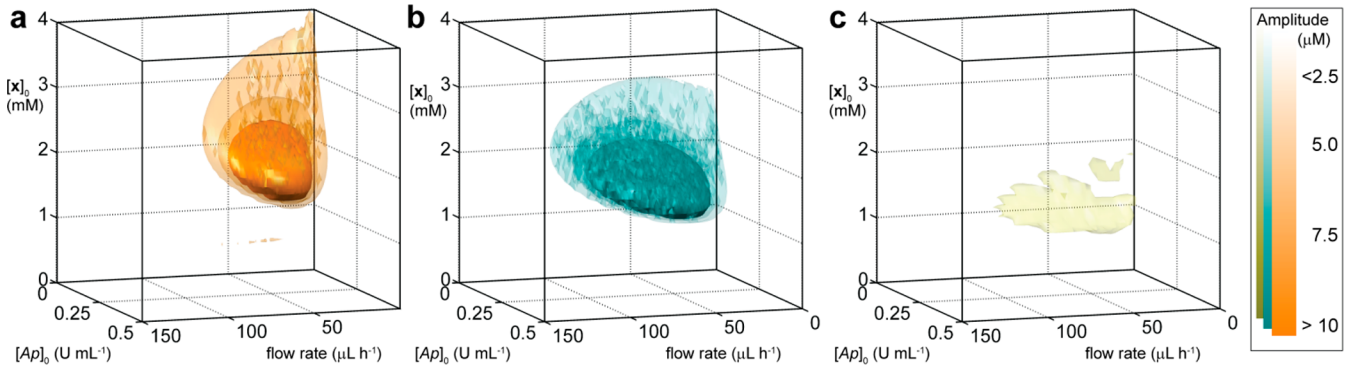

Figure 3. Conditions for sustained oscillations for pro-inhibitors **2**–**4** predicted by mathematical modeling. The colored areas, orange in (a) for **2**, cyan in (b) for **3**, green in (c) for **4**, represent the oscillatory regime above a threshold of 2.5 μM which is based on varying conditions of flow rate, $[Ap]_0$, and $[x]_0$ (with x = **2**, **3**, **4**) from 0 to 150 μL h^{-1}, 0–0.5 U mL^{-1}, and 0–5 mM, respectively. The increasing color intensities indicate increasing peak-to-peak amplitudes of the oscillations.

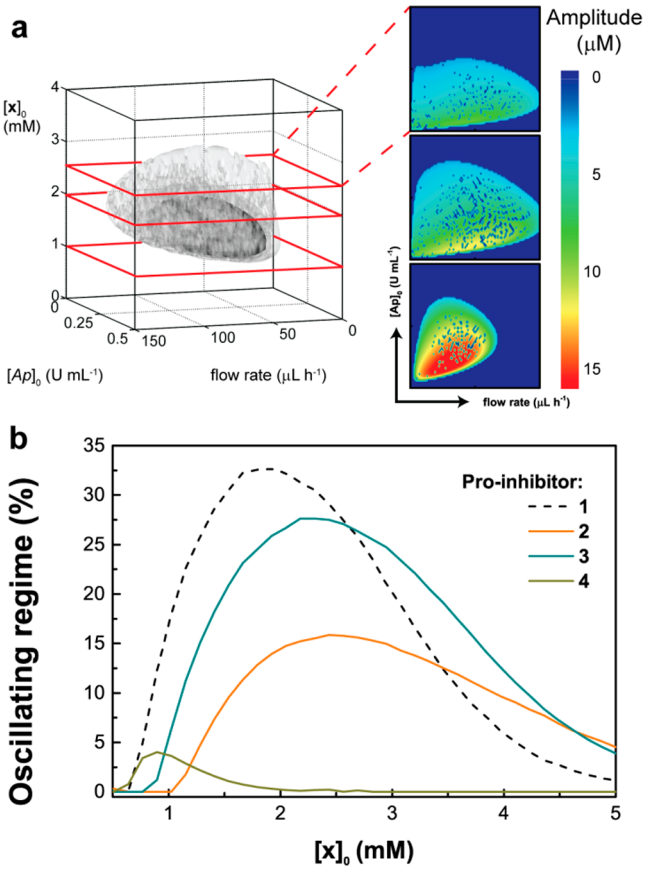

Figure 4. Optimal condition screening procedure (a) shown by dividing a 3D phase plot of **1** into multiple (flow, Ap)-phase planes. At each grid of $[x]_0$, slices of (flow, Ap)-phase planes were analyzed for the presence of an oscillating regime (non-blue area, x μL h^{-1} × y U mL^{-1}), within the screened space (blue area, 150 μL h^{-1} × 0.5 U mL^{-1}). This procedure is repeated for each pro-inhibitor, and (b) the analysis is summarized by plotting the relative area of oscillatory regimes in (flow, Ap)-phase against $[x]_0$, showing the apparent optimal $[x]_0$ for each pro-inhibitor. In contrast to the 3D phase plots, the thresholds are removed to show full domain of $[x]_0$ under which sustained oscillations can be found.

of the network did not lead to corresponding changes in network characteristics such as period or amplitude.

Instead, each pro-inhibitor required a different set of conditions (flow, $[Ap]_0$, $[x]_0$) in order to re-establish the "programmed" network behavior of sustained oscillations. For compound **4**, the Z-Gly modified pro-inhibitor, the predicted regime for sustained oscillations was very small and amplitudes very low. For this pro-inhibitor, no sustained oscillatory behavior was found. It is important to note that by changing the set of conditions (flow, $[Ap]_0$, $[x]_0$) the limit cycles become different, and at every time point, the combination of concentrations for all the small molecules (pro-inhibitor, intermediate inhibitor, and AEBSF) as well as trypsin are different for each network. Effectively, our results show that networks with the same topology, and the same components, but slightly different molecular structures, will have different regimes where sustained oscillations will be found. These findings have important implications for the future design of complex molecular networks, as they imply that the desired output of a network under certain conditions can be found by choosing the appropriate small molecules and associated reaction rates. We envision that these studies contribute to the forward engineering of out-of-equilibrium networks with robust and tunable outputs.

EXPERIMENTAL SECTION

Synthesis. Pro-inhibitors were synthesized by coupling commercially available 4-(2-aminoethyl)benzenesulfonyl fluoride (AEBSF, active inhibitor) to peptide cores functionalized with different R groups. The strategy combines standard peptide coupling in both solution-phase and Fmoc solid-phase peptide protocol on a trityl resin.[34] Full details of the synthesis and characterization of all compounds appear in the Supporting Information ESI-S2.

Kinetic Studies. Isolated reactions for the activation step were studied by mixing varying concentrations of pro-inhibitor with Tr. Under standardized conditions (100 mM Tris-HCl, pD 7.7, 20 mM $CaCl_2$ in D_2O at 23 °C), conversions of different pro-inhibitors into intermediate inhibitor were followed in time by ^{1}H NMR. Initial speeds of the reaction at different concentration levels were used to construct Lineweaver–Burk plots, from which the kinetic parameters k_{cat} and K_M (and thus k_{act}) could be obtained. Full details on the determination of kinetic parameters, including those for background reactions, appear in Supporting Information ESI-S3.

Batch Experiments. For experiments in batch conditions, **1**–**4** (260 μM) were mixed with Tg (130 μM), Tr (23 μM), and Ap (0.830 U mL^{-1}) in 100 mM Tris buffer, pH 7.7, containing 20 mM $CaCl_2$ at 25 °C. Aliquots of the reaction mixture were diluted with an aqueous 0.1 M $KHSO_4$ (10 times aliquot volume) solution to quench all reactions.

Flow Experiments. A typical continuous stirred tank reactor (CSTR) experiment is fed by four separate inlets to supply Tg (333

DOI: 10.1021/jacs.5b08129
J. Am. Chem. Soc. 2015, 137, 12415–12420

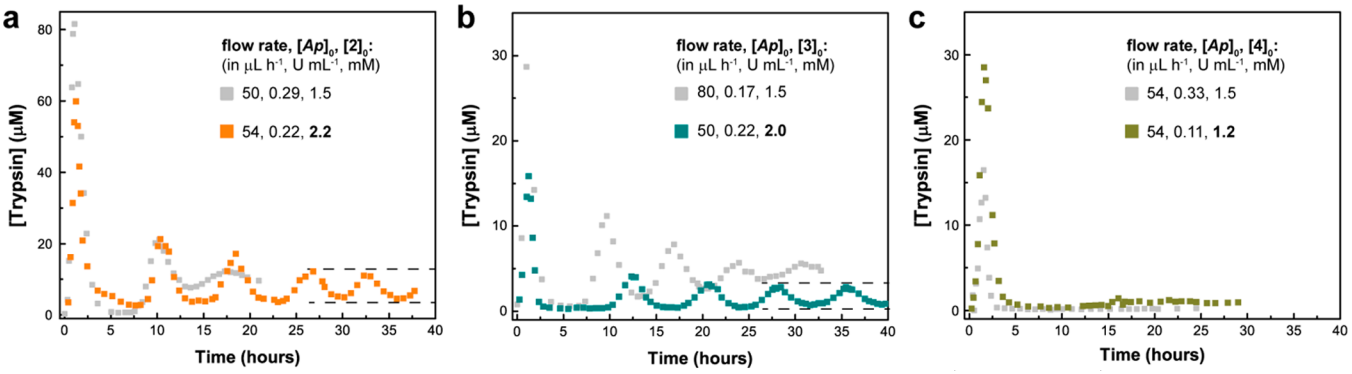

Figure 5. Experimental time series conducted under conditions found by the analysis shown in Figure 4 (colored squares) compared with time series under initial conditions from Figure 1c (gray squares) for (a) **2**, (b) **3**, and (a) **4**. The oscillatory states in (a) and (b) are indicated with dashed lines.

μM in HCl, $CaCl_2$ 4:36 mM), Tr (27 μg/mL, 1.16 μM in Tris-HCl, $CaCl_2$ 500:20 mM, pH 7.7), Ap (1.7−3.3 U mL^{-1} in Tris-HCl, $MgCl_2$ 10:10 mM, pH 7.7), and **1**−**4** (6−11 mM in HCl 2 mM). The 250 μL poly(dimethylsiloxane) (PDMS) reactor is kept at 24 °C. The different reagents were flown in with fractions of the total flow rate (0.5, 0.2, 0.2, and 0.1 for Tg, Tr, Ap, **1**−**4** respectively), leading to initial concentrations in the reactor of Tg (0.167 mM), Tr (0.00023 mM), Ap (0.17−0.33 U mL^{-1}), **1**−**4** (1.2−2.2 mM) with 100 mM Tris-HCl, pH 7.7, 20 mM $CaCl_2$, 1 mM $MgCl_2$ as the final buffer solution. Aliquots of the reaction mixture were diluted with 150 μL of an aqueous 0.1 M $KHSO_4$ solution to quench all reactions.

Details on the fabrication of PDMS reactors are reported in Supporting Information ESI-5. For additional information on the preparation of solutions, and the stability thereof, we refer the reader to the Supporting Information of previous work.[17]

Trypsin Activity Assay. Trypsin activity was measured by mixing 150 μL of the quenched reaction mixture with 3 mL of 5 μg/mL bis(Cbz-L-Arg)-rhodamine fluorogenic substrate in 50 mM Tris-HCl, pH 7.7. The increase in fluorescence intensity (λ_{ex} = 450 nm, λ_{em} = 520 nm) was monitored for 40 s, and the initial, linear slope was compared to a calibration curve to find the concentration of active trypsin.

Computational Screening Analyses. Bifurcation diagram and computational screening process for initial conditions in our flow experiments are both based on a so-called end-state analysis (see ESI-S4.1). The methods use a previously reported mathematical model based on mass action kinetics.[17] The output of both methods is shown in Figures 2−4, with the borders of used parameter spaces defined in the captions of corresponding figures. For further details, and computer scripts used for the analyses, see Supporting Information ESI-S4.

■ ASSOCIATED CONTENT

Supporting Information

The Supporting Information is available free of charge on the ACS Publications website at DOI: 10.1021/jacs.5b08129.

Chemical compound information, kinetic data, computational analyses, and scripts (PDF)

■ AUTHOR INFORMATION

Corresponding Author

*w.huck@science.ru.nl

Present Address

†Department of Chemistry and Chemical Biology, Harvard University, 12 Oxford Street, MA 02138.

Notes

The authors declare no competing financial interests.

■ ACKNOWLEDGMENTS

We thank Britta Helwig for supporting experimental work. Our work is supported by the European Research Council (ERC; Advanced Grant 246812 Intercom (W.T.S.H.)), The Netherlands Organization for Scientific Research (NWO, VICI Grant 700.10.44 (W.T.S.H.)), and funding from the Dutch Ministry of Education, Culture and Science (Gravity program 024.001.035).

■ REFERENCES

(1) Kholodenko, B. N. *Nat. Rev. Mol. Cell Biol.* **2006**, *7*, 165−176.
(2) Mohawk, J. A.; Green, C. B.; Takahashi, J. S. *Annu. Rev. Neurosci.* **2012**, *35*, 445−462.
(3) Barabási, A.-L.; Oltvai, Z. N. *Nat. Rev. Genet.* **2004**, *5*, 101−113.
(4) Karsenti, E. *Nat. Rev. Mol. Cell Biol.* **2008**, *9*, 255−262.
(5) Goldbeter, A.; Gérard, C.; Gonze, D.; Leloup, J.-C.; Dupont, G. *FEBS Lett.* **2012**, *586*, 2955−2965.
(6) Novák, B.; Tyson, J. J. *Nat. Rev. Mol. Cell Biol.* **2008**, *9*, 981−991.
(7) Ferrell, J. E.; Tsai, T. Y.; Yang, C. Q. O. *Cell* **2011**, *144*, 874−885.
(8) Kim, J.; Winfree, E. *Mol. Syst. Biol.* **2011**, *7*, 465.
(9) Purcell, O.; Savery, N. J.; Grierson, C. S.; di Bernardo, M. *J. R. Soc., Interface* **2010**, *7*, 1503−1524.
(10) Elowitz, M. B.; Leibler, S. *Nature* **2000**, *403*, 335−338.
(11) Hasty, J.; McMillen, D.; Collins, J. J. *Nature* **2002**, *420*, 224−230.
(12) Boekhoven, J.; Poolman, J. M.; Maity, C.; Li, F.; van der Mee, L.; Minkenberg, C. B.; Mendes, E.; van Esch, J. H.; Eelkema, R. *Nat. Chem.* **2013**, *5*, 433−437.
(13) Malakoutikhah, M.; Peyralans, J. − J. P.; Colomb-Delsuc, M.; Fanlo-Virgós, H.; Stuart, M. C. A.; Otto, S. *J. Am. Chem. Soc.* **2013**, *135*, 18406−18417.
(14) Pappas, C. G.; Sasselli, I. R.; Ulijn, R. V. *Angew. Chem., Int. Ed.* **2015**, *54*, 8119−8123.
(15) Lentini, R.; Forlin, M.; Martini, L.; Del Bianco, C.; Spencer, A. C.; Torino, D.; Mansy, S. S. *ACS Synth. Biol.* **2013**, *2*, 482−489.
(16) Salis, H. M.; Mirsky, E. A.; Voigt, C. A. *Nat. Biotechnol.* **2009**, *27*, 946−952.
(17) Semenov, S. N.; Wong, A. S. Y.; Van der Made, R. M.; Postma, S. G. J.; Groen, J.; Van Roekel, H. W. H.; De Greef, T. F. A.; Huck, W. T. S. *Nat. Chem.* **2015**, *7*, 160−165.
(18) Karzbrun, E.; Tayar, A. M.; Noireaux, V.; Bar-Ziv, R. H. *Science* **2014**, *345*, 829−832.
(19) Montagne, K.; Plasson, R.; Sakai, Y.; Fujii, T.; Rondelez, Y. *Mol. Syst. Biol.* **2011**, *7*, 466.
(20) Padirac, A.; Fujii, T.; Estévez-Torres, A.; Rondelez, Y. *J. Am. Chem. Soc.* **2013**, *135*, 14586−14592.
(21) Nakajima, M.; Imai, K.; Ito, H.; Nishiwaki, T.; Murayama, Y.; Iwasaki, H.; Oyama, T.; Kondo, T. *Science* **2005**, *308*, 414−415.
(22) Zieske, K.; Schwille, P. *Angew. Chem., Int. Ed.* **2013**, *52*, 459−462.

DOI: 10.1021/jacs.5b08129
J. Am. Chem. Soc. 2015, 137, 12415−12420

(23) Epstein, I. R.; Showalter, K. *J. Phys. Chem.* **1996**, *100*, 13132−13147.
(24) Zaikin, A. N.; Zhabotinsky, A. M. *Nature* **1970**, *225*, 535−537.
(25) De Kepper, P.; Epstein, I. R.; Kustin, K. A. *J. Am. Chem. Soc.* **1981**, *103*, 2133−2134.
(26) Kurin-Csörgei, K.; Epstein, I. R.; Orbán, M. *Nature* **2005**, *433*, 139−142.
(27) Huber, R.; Bode, W. *Acc. Chem. Res.* **1978**, *11*, 114−122.
(28) Abita, J.-P.; Delaage, M.; Lazdunsk, M.; Savrda, J. *Eur. J. Biochem.* **1969**, *8*, 314−324.
(29) Powers, J. C.; Asgian, J. L.; Ekici, D. Ö.; Ellis James, K. *Chem. Rev.* **2002**, *102*, 4639−4750.
(30) Seely, J. H.; Benoiton, N. L. *Can. J. Biochem.* **1970**, *48*, 1122−1131.
(31) Vandermarliere, E.; Mueller, M.; Martens, L. *Mass Spectrom. Rev.* **2013**, *32*, 453−465.
(32) Epstein, I. R.; Pojman, J. A. *An Introduction To Nonlinear Chemical Dynamics*, 1st ed.; Oxford University Press: New York, Oxford, 1994.
(33) Strogatz, S. H. *Nonlinear Dynamics and Chaos*, 1st ed.; Westview Press: Cambridge, MA, 1994.
(34) Fields, G. B.; Noble, R. L. *Int. J. Pept. Protein Res.* **1990**, *35*, 161−214.

DOI: 10.1021/jacs.5b08129
J. Am. Chem. Soc. 2015, 137, 12415−12420